TECHNOLOGIES RESOURCES RESERVES DEMAND

IMPACT CONSERVATION MANAGEMENT POLICY

The International Journal

Available online at www.sciencedirect.com

ScienceDirect

https://www.sciencedirect.com/science/article/pii/S0360544218321790

Rapid emulsification of a fuel–water rapid internal mixing injector for emulsion fuel combustion

Aizam Shahroni Mohd Arshad, Yuzuru Nada*, Yoshiyuki Kidoguchi, Daisuke Asao and Shinichiro Yoshimura

Department of Energy System, Tokushima University, 2-1 Minami-Josanjima, Tokushima 770-8506, Japan

*Corresponding author:

Yuzuru Nada

Department of Energy System, Tokushima University, 2-1 Minami-Josanjima, Tokushima 770-8506, Japan

E-mail address: ynada@tokushima-u.ac.jp

Declarations of interest: none

Abstract

In this study, a fuel–water rapid internal mixing injector capable of reducing emissions from combustion furnaces operating under high load conditions was developed. Employing this injector allows the injection of a fresh emulsified fuel mixture without requiring surfactants or additional processing equipment. The aim of the present study was to investigate the emulsification, atomization, and emission performance of the injector when using soybean oil as a model high-viscosity fuel from a renewable source. Successful emulsification was observed in the mixing chamber over a wide range of water content ratios up to 0.5, under which a water-in-oil emulsion was discharged from the injector. As the water content ratio was increased, the Sauter mean diameter of the droplets in the spray increased. This is a result of the decrease in the mass flow ratio of atomizing gas to liquid and the increase in the viscosity of the fuel emulsion. Although the emulsification of the base fuel resulted in the discharge of large droplets, the results showed that the nitrogen oxide and particulate matter emissions from a combustion furnace incorporating the injector were found to be reduced simultaneously following the introduction of water even under a high combustion load.

Keywords: Fuel–water rapid internal mixing injector; Emulsification; Atomization; Combustion; Soot; NO_x

1. Introduction

Population growth and industrial expansion have led to tremendous increases in human activity, mostly driven by energy derived from fossil fuels; however, the supply of fossil fuels is finite and will soon be depleted. In addition, pollutant emissions from the combustion of fossil fuel are the main cause of numerous global problems, such as the greenhouse effect, ozone depletion, acid rain, environmental pollution, and human health problems. To address the issue of pollutant emissions, particularly nitrogen oxides (NO_x) and soot, many strategies for the reduction of the generation of these hazardous substances have been developed and adopted. With increasing concern over these issues, previous research on pollutant emissions has also revealed new technologies that can be used to provide a cleaner environment for various combustion systems. These include moderate or intense low-oxygen dilution (MILD) combustion [1], low-temperature combustion [2], and oxy-fuel combustion [3]. MILD combustion is an effective technology for the simultaneous reduction of NO_x and soot emissions [4].

Over the last several decades, water emulsification, which is the mixing of a base fuel and water with or without the presence of surfactants, has been a well-known technique that can be used to simultaneously suppress NO_x and soot emissions in practical combustion systems [5]. When water-emulsified fuel is injected into a region already containing hot gases, the flash evaporation of the very small water droplets dispersed in the emulsified fuel results in secondary atomization [6–8], thus generating a large number of even smaller droplets [9]. This flash evaporation also enhances the mixing of the fuel vapor with the ambient air [10, 11] and increases the concentration of OH radicals, effectively reducing soot emission [5, 12, 13]. The introduction of water also reduces NO_x emissions [14–16] because the flame temperature is reduced by the latent heat of the water as well as a dilution effect associated with the generation of water vapor [17]. Furthermore, Dryer et al. [18] have suggested that

the added water may influence NO_x formation via an increase in the number of OH radicals, leading to a reduction in the oxygen atom concentration and hence the suppression of NO_x formation [19].

The application of emulsified fuel also improves the quality of atomization through secondary atomization mechanisms such as micro-explosion and puffing. Even when high-viscosity oil including vegetable oil is supplied to a burner, fine droplets are generated in the regions of hot gas near the flames. This likely contributes to the stabilization of the combustion [13] and consequently extends the efficiency of conventional burners supplied with high-viscosity oil. The emulsification of fuel is therefore a countermeasure against the depletion of fossil fuels.

However, emulsified fuel combustion has some disadvantages. Emulsification requires the use of expensive surfactants. Ghannam and Selim [20] have reported that a surfactant is required in the formation of fuel–water emulsions to avoid coalescence. However, the addition of surfactant to emulsion preparation has shown a difficulty to maintain its stability due to deterioration of the emulsified fuel over time [20, 21]. Furthermore, temperature lowering in a flame frequently induces unstable combustion in some situations. Spadaccini and Pelmas [22] have reported that they were able to maximize the combustion efficiency by optimizing the water content in their emulsified fuel and that the use of an emulsified fuel containing excess water destabilized the flame. Because the stability of the flame is significantly affected by the thermal conditions, such as the wall temperature of the combustion furnace, it is desirable for the operator to immediately adjust the water content in emulsified fuel in response to thermal conditions to optimize the combustion efficiency.

To overcome these disadvantages, our research group has developed an injector incorporated with a small chamber in which the base fuel introduced into the injector is rapidly mixed with water by the swirling flow of air. Because the base fuel would be

emulsified during this mixing process, additional emulsification equipment [14, 16] and surfactants [20] are not required. If the emulsification of base fuel is achieved in the chamber, fresh emulsified fuel will be constantly being supplied into the furnace. In addition, the water content in the emulsified fuel mixture can be optimized in response to the particular combustion conditions during furnace operation. The optimization of the water content supplied by the injector could therefore contribute to the stable operation of combustion furnaces.

In the present study, the emulsification and atomization characteristics of an injector were investigated with high-viscosity vegetable oil used as fuel. The internal structure of the droplets discharged from our injector was examined by microscopy over a wide range of water contents to determine whether emulsification was successfully achieved. A spray droplet size measurement system based on the shadowgraph method was employed to examine the atomization characteristics including the mean diameter of the droplets discharged from the injector. Finally, the performance of the injector in terms of the reduction of NO_x and particulate matter (PM) emissions from a laboratory-scale combustion furnace operating under high-load conditions was assessed.

2. Experimental setup

2.1. Injector and liquid supply system

Figs. 1(a) and (b) shows cross-sectional and exploded-view diagrams, respectively, of the fuel–water rapid internal mixing (RIM) injector used in the experiments. The injector consists of a main body, a swirler, a mixing chamber, and a cover clamping the mixing chamber onto the main body, all of which are made of brass. The length of the injector is 107 mm, and the mixing chamber is 33 mm in length and 12.6 mm in diameter. The base fuel, water, and atomizing air are respectively introduced into the mixing chamber through a coaxial slit with

a slit size of 0.45 mm, a central channel with a diameter of 2 mm, and a four-slit swirler with an angle of inclination of 30°, generating rotational flow within the chamber. The introduced fuel and water are set into motion and mixed by the swirling air, resulting in the emulsification of the fuel within the chamber. The emulsified fuel is subsequently discharged through eight holes of 1.0 mm in diameter arranged in a circular pattern in the upper section of the chamber. Each injection hole is inclined by 45° relative to the vertical direction.

In recent years, our research group has been working on the development of an RIM injector that can atomize high-viscosity fuels. Soybean oil was selected as a base fuel because it is a good representative high-viscosity vegetable oil which can also be easily procured from a local supplier in Japan at a low cost. Recently, our interest in the potential of utilizing high-viscosity fuels in burner combustion systems equipped with injectors has come to focus on more highly viscous oils, such as mineral oil and heavy fuel. Results obtained using more highly viscous oil will be reported in a future publication.

The properties of the soybean oil used in this study are listed in Table 1. The viscosity of the pure soybean oil was measured using a viscometer (Rion, VF-04F) and was found to be 52 mm^2/s at 25 °C, which is 17 times higher than that of conventional light oil (approximately 3 mm^2/s). Unfortunately, Table 1 does not include the properties of the emulsified fuel discharged from the proposed injector. The base fuel and water were injected independently into the mixing chamber, where rapid emulsification occurs by the atomizing air without the presence of a surfactant; thus, the emulsified fuel discharged from the injector has a short lifetime, which makes the investigation of its properties difficult. Therefore, the variation in the properties of the emulsified fuel with the water content ratio could not be measured.

A trochoid pump (Nippon Oil Pump, TOP-1ME75-1-10MAVB) was used to supply the high-viscosity oil to the injector. The water and atomizing air were supplied by a magnet

pump and a compressor, respectively. The mass flow rates of the oil, water, and air were controlled by needle valves in conjunction with a mass flow meter (OVAL, CoriMate II CR003) for the oil and calibrated rotameters (KOFLOC, RK1200) for the air and water.

2.2. Internal structure of discharged droplets

To examine the fuel emulsification resulting from the mixing in the chamber, the internal structure of the droplets discharged from the injector was investigated. This was done using a small shallow dish filled with silicon oil that was inserted into the spray stream for 1 s at a point 143 mm downstream from the injection hole, during which time several large droplets from the spray were captured in the pool of silicon oil. These droplets were observed using a digital microscope (KEYENCE, VH-Z25) within 1 min of sampling. During the droplet sampling trials, red and blue coloring agents were added to the soybean oil and water, respectively, in the injector to allow for the easy identification of water and oil droplets in the microscopic images. The spatial resolution of the images captured by the microscope is 1.25 μm/pixel.

It should be noted that the sampling procedure employed here had at least two inherent drawbacks that likely introduced significant errors and thus make quantitative assessment difficult. The first effect is that the capture method preferentially traps droplets with large diameters because they have sufficient inertia to reach the pool. Second, the distribution of internal droplets present in the emulsion droplets shows temporal variation because of the coalescence among internal droplets in the absence of a surfactant. Nevertheless, direct observations of the captured droplets via a microscope can still provide important information regarding the internal structure, including the type of emulsification.

To investigate the mechanism of fuel emulsification in the mixing chamber of the injector, the fuel and water streams in a mixing chamber composed of transparent acrylic were

observed using a high-speed camera (Nobby Tech. Ltd., Phantom V13) with a frame rate of 3000 fps and an exposure time of 30 μs. The spatial resolution of the captured images is 69 μm/pixel.

2.3. Size of droplet in sprays

The Sauter mean diameters (SMDs) of droplets in sprays discharged from the injector were evaluated using shadowgraph images. Fig. 2 shows a schematic of the shadowgraph system, which consists of a spray chamber and an injector as well as a nano-spark photography unit [23] and a digital camera. The spray chamber is a cube with a height of 190 mm and a square cross section of 180 mm × 180 mm. The injector was installed at the upper surface of the chamber and inclined obliquely downward at 45°, such that the spray from a single hole was injected downward into the chamber while the sprays from the remaining holes were expelled into a separate area. This was performed to concentrate the investigation on a single spray and to avoid interference from other sprays.

The chamber has two optical windows composed of silicate glass on opposing lateral sides to allow parallel light emitted by a light source to pass through and illuminate the spray in the chamber. Illumination was provided for short durations of 30 ns. Shadowgraph images of the spray were captured using a digital camera (Nikon D7000) with an ISO speed of 100 and a spatial resolution of 4.1 μm/pixel. With this system, static images of droplets moving with high velocities on the order of 100 m/s could be obtained. The diameters of droplets in the sprays were measured by processing images captured in this way. The size of each image is 20 mm × 13 mm, and the top of the image region is shifted 10.5 mm downstream from the injection hole.

In the image processing, the radius of each droplet was evaluated as a distance from luminosity centroid of droplet to the position where the luminosity was intermediate between

luminosity centroid and the outer region surrounding the droplet. The evaluated diameters of the droplets were corrected based on the correlation between the diameters evaluated using this method and the corresponding actual diameters. This correlation was obtained from shadowgraph images of a glass plate on which approximately 1000 glass balls with various diameters were scattered, simulating droplets in a spray. The actual diameter of every ball was manually measured using enlarged images captured by a microscope. A linear correlation between the evaluated diameter D_0 and the actual diameter D was obtained, as shown in Fig. 3. The slope of the correlation line is 1.12, indicating that the actual diameter is 1.12 times the evaluated diameter. The error in the evaluated diameter with respect to the actual diameter is within 12%. More than 5000 droplets were extracted from the images to calculate the SMD and the probability distribution of the diameter.

2.4. NO_x and soot emissions

In this study, NO_x, CO, and soot emissions from a laboratory-scale furnace with the injector incorporated were measured to assess the effectiveness of the injector in reducing the emissions. Fig. 4 shows a schematic of the combustion test apparatus, which consists of a combustion furnace and an injector as well as a NO_x, CO, and soot measurement system. The furnace used in this study is 1400 mm in length, which is more than twice the length of the luminous flame within the furnace.

The RIM injector was surrounded by a cylindrical flame holder with an inner diameter of 95 mm, which plays an important role in the anchoring of spray flames, thus sustaining combustion under excess water conditions. Fig. 5 shows a schematic of the flame holder. There are a large number of holes at the bottom of the holder, through which secondary air was supplied to the holder. Fuel spray was injected toward the side wall of the flame holder at an angle of 45° with respect to the horizontal. After combustion tests, it was confirmed that

there were no carbon deposits attached to the wall. Whereas the RIM injector incorporates a small swirler inside the mixing chamber to mix the base fuel with water, the holder itself has no swirler. Thus, the swirling flow appearing in the flame holder is very weak because the injection holes are drilled perpendicularly into the wall of the mixing chamber; consequently, the effect of the swirling flow on the experimental results is negligible.

The secondary air mass flow rate was determined using a laminar flow meter (Yamada, LFM-8). A propane pilot burner situated close to the injector was used to ignite the soybean oil spray. In addition, a water-cooled probe with an inner diameter of 1 mm was inserted into the furnace exit, through which the flue gas was withdrawn via suction at a flow rate of 0.4 L/min. The NO_x and CO concentrations in the flue gas were measured by a gas analyzer (Horiba, PG-250). PM in the flue gas sampled by another probe with a diameter of 10 mm was collected on a piece of filter paper, and the weight of the PM on the paper was determined using an electronic scale (METTLER, AE240). Following this measurement, the soluble organic fraction (SOF) in the PM was removed by Soxhlet extraction, and the residual mass corresponding to dry soot (SOLID) was determined, again using an electronic scale. The weight of the SOF component was calculated as the difference between the masses of PM and SOLID. To investigate the difference between the structures of soot samples collected under various water content conditions, transmission electron microscopy (TEM; JEM-2100F, JEOL) at 200 kV and a magnification of 50000 was performed. The spatial resolution of the captured TEM images is 0.29 nm/pixel.

The temperature profiles in the combustion furnace were measured using R-type thermocouples to assess the relationship between the temperature and NO_x emissions. In this study, a cylindrical coordinate system (x, r) with its origin positioned at the same height as the injection holes along the center line of the injector was used. The vertical profile at r = 0 mm was measured from x = 167 mm, just above the flame holder, to x = 617 mm. The radial

profile was measured at x = 42 mm inside the flame holder, as shown in Fig. 5. The thermocouples used during the experimental trials have a diameter of 0.1 mm and a width of 1 mm and are coated with yttrium–beryllium oxide to prevent a catalytic reaction [24]. The mean temperature was obtained by averaging the instantaneous measured temperature over a span of 60 s. Radiative heat loss correction [25] was not applied to the results obtained from the thermocouple measurements because no information regarding the gas velocity distributions in the furnaces is available, and thus the temperatures presented in this paper include some error introduced by radiative heat loss. However, the heat loss has a weak influence on the differences among the temperatures at different water content ratios because the furnace has a similar velocity distribution regardless of the water content ratio, which is almost completely determined by the configuration in the lower section of the combustion furnace (see Fig. 5).

The flame appearance was captured using a digital camera (Nikon D7000) operated with a shutter speed of 1/125 s, an ISO sensitivity of 400, and an aperture of f3.5. The furnace was fitted with a rectangular window with dimensions of 20 mm × 1000 mm for the observation and imaging of the flames. The experiment was performed in a dark room to reduce noise in the images.

2.5. Experimental conditions

During the assessment of the spray and emulsification characteristics, the mass flow rate of the water, M_w, was varied from 0 to 2.61 kg/h while a base fuel mass flow rate M_f of 1.13 ± 0.02 kg/h and an atomizing gas flow rate M_a of 3.98 ± 0.07 kg/h were maintained at an injection pressure of 0.3 MPa. In the present study, the extent of water introduction is represented by the water content ratio $Y_w = M_w/(M_f + M_w)$. During the experimental trials, this

ratio was varied from 0 to 0.7 with a maximum error of ±2.0%. Nitrogen was used as the atomizing gas rather than air for safety reasons.

During the measurements of NO_x, CO, and soot emissions from the combustion furnace, the flow rates of the base fuel, atomizing air, and water were set to the same values as those applied during the spray measurements. The mass flow rate of the secondary air was maintained at 11.44 ± 0.29 kg/h. The equivalence ratio ϕ, which was evaluated from the measured elemental composition listed in Table 1, was 0.9 with a maximum error of 0.02 under the above conditions. During soot emission assessments, the mass flow rate of the base fuel was increased to 1.31 kg/h (ϕ = 1.05) to simulate the combustion conditions in a conventional furnace operating under high-load conditions.

3. Results

3.1. Emulsification in the mixing chamber of the rapid internal mixing injector

Fig. 6 shows microscopic images of droplets sampled at Y_w = 0, 0.3, 0.5, and 0.7. When only pure fuel was introduced (Fig. 6(a)), many fuel droplets trapped in the silicon oil, observable as red particles, were present in the images. Almost all droplets shown in Fig. 6(a) are very large with diameters exceeding 50 μm. This is because the sampling method used in this study preferentially collects large droplets. For Y_w = 0.3 (Fig. 6(b)), the red droplets in the images appear to contain smaller blue droplets within them, which are water droplets dispersed in the base fuel. This image demonstrates that the injector successfully emulsified the base fuel without any surfactants. Because the water droplets are dispersed in the base fuel, the discharged emulsified fuel may be classified as a water-in-oil (W/O) emulsion under these conditions.

As the water content ratio was increased up to 0.5, the emulsified fuel sustained the structure of a W/O emulsion even though the diameter of the droplets increased. It is evident

from these images that the injector can achieve rapid emulsification over a wide range of water content ratios within the brief time interval during which the base fuel passes through the mixing chamber. The effects of the water content ratio on the droplet diameter will be explained in the following section. In contrast, at a water content of 0.7, many droplets of pure water appeared with some droplets of emulsified fuel. The occurrence of incomplete emulsification indicates that there is an upper limit to the water content at which the injector can successfully emulsify the base fuel.

The emulsification mechanism occurring in the mixing chamber is explained here by referring to movies captured using the high-speed camera. Fig. 7 shows a series of successive photographic images of the transparent mixing chamber during the introduction of the base fuel alone ($Y_w = 0$). The location of the depicted region is indicated by the broken line in Fig. 7(a), in which the red and green arrows respectively denote the flow directions of the fuel and atomizing gas. Spiral streams of fuel and the formation of a film of fuel on the inside wall of the mixing chamber were observed in these images. This film is formed as the swirling motion of the atomizing gas is imparted to the fuel introduced from the central channel and the swirling fuel impinges on the inside wall. Eventually, the fuel is discharged from the holes arranged in the chamber.

Fig. 8 shows another series of successive images of the mixing chamber for a trial during which water was introduced at a water content ratio of $Y_w = 0.3$. Images for the other cases are omitted because the behavior of the emulsified fuel in the mixing chamber was similar to that at $Y_w = 0.3$. What is interesting about these observations is that as soon as water was introduced, the mixing chamber appeared to fill with a milky liquid that was subsequently discharged from the injection holes. This indicates that the emulsification of base fuel starts immediately after the injection of water into the mixing chamber. Fig. 9 shows successive images captured by the high-speed camera using the injector with the mixing chamber

dismounted. These images show liquid flows near the outlets of the coaxial slit and central channel (see Fig. 1). Fuel and water expelled from the outlets were atomized by the swirling flow of atomizing gas. During the process, the liquids mixed with one another, resulting in the emulsification of the base fuel with water. Fig. 10 shows microscopy images of droplets discharged from both outlets. Many droplets of pure water were observed, though some emulsified fuel droplets were also present. This partial emulsification is a result of the short mixing time near the outlets. The remaining water subsequently became mixed with the base fuel in the mixing chamber.

From the results shown in Figs. 7–10, the mechanism of emulsification was inferred to be as follows. The separately introduced base fuel and water are mixed near the outlets of flow channels with the assistance of the strong swirling motion of the atomizing gas; at this time, part of the base fuel is emulsified with water. The gas flow then simultaneously atomizes the emulsified fuel and the water, and the resulting droplets impinge on the inner wall of the mixing chamber. As the fuel and residual water travel through the mixing chamber to the injection holes, they are mixed again, and well-emulsified fuel is then discharged from the chamber. As shown in Fig. 8, the view to the inside of the mixing chamber was impeded by emulsified fuel attached to the side wall of the transparent chamber. However, the flow pattern of the emulsified fuel is similar to the pure fuel flow exhibited in Fig. 7. Li et al. [26] recommended using the map developed by Oshinowo and Charles [27] to predict the flow regimes inside internal mixing chambers. According to the criterion by Oshinowo and Charles [27], the flow regimes under the present experimental conditions are classified as annular flows because of the high volume flow rate of the atomizing gas and the high Froude number. Therefore, the mixing of fuel with water in the injector likely occurs in the thin film.

3.2. Atomization characteristics of the rapid internal mixing injector

Fig. 11(a) shows the diameter distribution characteristics of spray droplets of the tested fuel discharged from the injector at various water content ratios. The corresponding SMDs are plotted against the water content ratio and the gas-to-liquid mass ratio (GLR) in Fig. 11(b). In the case of Y_w = 0, the diameter distribution had a peak at approximately 20 μm. Although the probability rapidly decreased with increasing diameter, several very large droplets with diameters exceeding 100 μm were generated under this condition, resulting in a large SMD value of 77 μm, as shown in Fig. 11(b). However, at Y_w = 0.3, the distribution was much broader. Under this condition, the peak for the small droplets was reduced, whereas that for the large droplets was increased, resulting in an increased SMD of 143 μm. When the water content ratio was increased from Y_w = 0.3 to 0.5, the diameter distribution graph was largely unchanged. This indicates that relatively few small fuel droplets were produced during the rapid emulsification. In contrast, when the water content ratio was increased from Y_w = 0.5 to 0.7, the proportion of fine droplets with diameters of less than 35 μm increased. Consequently, the SMD at Y_w = 0.7 decreased to 113 μm.

The formation of very large droplets when pure fuel was supplied can be explained in terms of the fuel streams in the mixing chamber. As shown in Fig. 7, the fuel film on the chamber wall was observed to form with an uneven thickness. When the thick portion of this film, indicated by arrows in Fig. 7, reached an injection hole, a significant quantity of fuel was discharged, generating the large droplets responsible for the high SMDs noted above.

As shown in Fig. 11(b), as the water content ratio was increased from 0 to 0.3, corresponding to a GLR of 2.47, the SMD increased by 46% (from 77 to 143 μm). This suggests that the decrease in the GLR associated with the increase in the water content ratio influences the deterioration of the atomization. In many previous studies [28–30], a similar trend of the SMD increasing with decreasing GLR has been reported. Another likely factor causing this increase in the SMD is the increase in viscosity resulting from the emulsification.

In previous studies [16, 31], it has been reported that the viscosity of emulsified fuel increases with increasing water content. The effects of viscosity on atomization have been discussed by Li at al. [28], who noted the influence of viscosity on the primary atomization in an internal mixing twin-fluid atomizer and concluded that a higher viscosity results in the production of much larger droplets. Together, these studies provide important insights into the influence of viscosity on the characteristics of the atomization. In contrast, a comparison of Fig. 11(a) and 11(b) reveals that the SMD decreased when the water content was increased from Y_w = 0.5 to 0.7 at low GLR of 1.05. This is likely related to the formation of pure water droplets, as shown in Fig. 6(d). As discussed above, at Y_w = 0.7, the base fuel is not completely emulsified. This implies that in a portion of the liquid film that forms on the inner wall of the chamber, the water is not sufficiently mixed with base fuel. Small droplets produced from this portion would be discharged because the viscosity of water is less than that of emulsified fuel. The probability shown in Fig. 11(a) includes the fine droplets of water; consequently, the SMD is low when pure water droplets are present.

It should be noted that our measurements regarding fuel droplets and emulsification were conducted under cold conditions. During actual combustion tests, the heat transferred to the mixing chamber, which is exposed in the furnace, may influence the emulsification and atomization characteristics of the spray droplets. This transferred heat would increase the temperature of the liquid present in the mixing chamber. Fig. 12 shows the variation in the viscosity of pure soybean oil with the oil temperature. The viscosity is seen to decrease with increasing oil temperature. During furnace operation, this decrease may promote the mixing of the base fuel and water in the chamber and improve the atomization of the emulsified fuel. Therefore, the SMD of the spray injected from the injector during furnace operation would be lower than that exhibited in Fig. 11. This is because the SMDs shown in Fig. 11 were measured with the temperature of the base fuel kept constant at 25 °C. However, the main

results described in the above sections, namely successful emulsification (Fig. 6) and the variation in the SMD (Fig. 11), are not qualitatively affected by this low-temperature operation because a decrease in the viscosity tends to promote emulsification and the increase in the SMD shown in Fig. 11 is attributable to the decrease in GLR and increase in viscosity resulting from emulsification.

3.3. Emissions from the combustion furnace incorporating the rapid internal mixing injector

This section discusses the assessment of the emissions from a furnace incorporating the developed injector. Combustion tests were conducted with water content ratios ranging from 0 to 0.7. Fig. 13 shows the variation in the CO concentration with the water content ratio. As shown in Fig. 11(b), the SMD increased with increasing water content ratio and eventually reached a maximum value of approximately 140 μm at Y_w = 0.5. In spite of the poor atomization, the combustion furnace incorporating the RIM injector could be stably operated for $Y_w \leq 0.5$. This is likely because of the generation of finer droplets by secondary atomization; as shown in Fig. 6, observation of the internal structure demonstrated the presence of emulsified droplets. As a result of the stable combustion, the CO concentration in the exhaust gas sampled from the furnace exit was approximately 0 ppm in this water content range (Fig. 13). In contrast, for $Y_w > 0.5$, the intermittent expulsion of large amounts of water vapor from the furnace exit was observed in conjunction with significant noise, possibly resulting from the oscillation of the flame. This unstable combustion is caused by the excess water forming pure water droplets, as shown in Fig. 6(d). As a result, the CO concentration rapidly increased up to 850 ppm at Y_w = 0.6 (Fig. 13). However, it should be noted that combustion at Y_w = 0.6 could be sustained even with such a high CO emission level. When the water content ratio was increased to 0.7, the CO concentration rapidly rose beyond 5000 ppm, and furnace operation was immediately stopped for safety reasons. From this, it is

reasonable to consider emulsified fuel at Y_w = 0.7 to be incombustible in this furnace. The upper limit of the water content ratio for stable furnace operation is therefore approximately 0.5 under the present experimental conditions.

Fig. 14 shows the appearance of the flame at Y_w = 0 and Y_w = 0.3. The axis in this figure represents the vertical distance from the injector holes. The flame at Y_w = 0 was observed to be brightly luminous, suggesting a strong soot propensity. In contrast, the presence of water at Y_w = 0.3 produced a darker flame color. In a previous study [32], the flame luminosity was expressed as a function of soot temperature and concentration. The change in the flame appearance indicates a decrease in the flame temperature and soot concentration.

Fig. 15 shows a plot of the NO_x emission index ($EINO_x$) as a function of the water content ratio during experimental trials with ϕ = 0.9. The $EINO_x$ values were estimated according to a definition proposed by Turns and Myhr [33]. This plot exhibits the same trend as that for conventional emulsified fuel combustion; the value of $EINO_x$ decreased with increasing water content ratio [16]. This is likely due to lower flame temperatures resulting from the latent heat of the added water [16, 20] and the pure dilution effect from the increase in the concentration of water vapor [17] and the depletion of oxygen atoms [18]. Fig. 16 presents vertical temperature distributions for Y_w = 0 and Y_w = 0.3. Vertical profiles under both conditions show similar trends, with the temperature peaking at x = 217 mm, and the difference between these peak temperatures is small at approximately 30 K. However, the difference at x = 167 mm, just above the flame holder, is larger (approximately 60 K), which means that temperature in the flame holder is significantly decreased by the addition of water. Fig. 17 shows the radial distribution of the temperature in the flame holder at x = 42 mm. As shown in Fig. 5, a larger radial component of the measurement position corresponds to a location nearer to the spray flame, and hence the peak temperature appears near the wall,

which is located at r = 42.5 mm. The peak temperature was decreased by approximately 100 K when water was added, which reduces the NO_x emissions, as shown in Fig. 15.

It is well known that NO_x production through the Zel'dovich mechanism is promoted above 1800 K. However, the temperatures in Figs. 16 and 17 are below 1800 K even at Y_w = 0. It should be noted that these temperatures are time-averaged. In the combustion furnace including the flame holder, the spray flame fluctuates temporally as a result of turbulence, and thus the temperature measured during the averaging time includes the temperatures of unburned mixtures. The actual temperature of the flame and burned gas in which NO_x is generated would be higher than the values given here.

Fig. 18 shows the PM, SOLID, and SOF mass concentrations measured at ϕ = 1.05 under various water content ratios. It should be noted that the present measurement system was unable to collect measurable quantities of PM at ϕ < 1.0, demonstrating the excellent performance of the injector with regard to reducing PM emission in furnaces operating under low load conditions. At ϕ = 1.05, the PM concentration significantly decreased with increasing water content, whereas the concentration of the SOLID component rapidly decreased. These results indicate that the injector is able to reduce SOLID emissions even under a high combustion load. The structure of the PM collected on the filters was observed using TEM. The TEM micrographs shown in Fig. 19 reveal that, regardless of the water content ratio, the collected PM is composed of conventional soot, the structure of which is a chain of fine particles with diameters of less than 50 nm. Thus, the reduction of the SOLID component is deemed to correspond to the reduction in soot emissions rather than that of cenospheres with diameters greater than 10 μm [9, 34].

The reduction in soot emissions may be attributable to several factors resulting from water addition. Nazha and Crookes [10] reported that the high-equivalence-ratio region that is present in emulsified fuel spray disappears as a result of the improved mixing of fuel vapor

with combustion air, which suppresses soot formation. Tue et al. [11] also reported that the enhanced mixing caused by the puffing behavior decreases the volume of the sooting region. Furthermore, Kadota and Yamasaki [5] have pointed out the important role of OH radicals in the oxidation of soot precursors in their review. However, it is difficult to identify the dominant factors responsible for the reduction of soot emission.

The SOF concentration slowly decreased with increasing water content ratio in the developed system, such that the PM released from the furnace at Y_w = 0.5 primarily consisted of the SOF. The emission of SOF components mainly originates from polycyclic aromatic hydrocarbons (PAHs) generated in the flame [12, 35]. Because the present combustion tests on PM emission were conducted under fuel-rich conditions, the residual fuel and PAHs remained in the exhaust gas. The remaining components were eventually discharged as soluble organic compounds without the formation of soot, and the SOF is therefore the predominant component of emitted PM at high water contents. The existence of the SOF component can be observed in the TEM images in Fig. 19. The outline of each particle at Y_w = 0.5 is somewhat unclear in this figure. This is likely because the particle is enveloped by a liquid corresponding to the SOF component.

As shown in Fig. 18, the decrease in the SOF component occurred more slowly than that in the SOLID component. In a previous study, Kozinski [12] presented the axial distribution of the concentration of PAHs. They demonstrated that the presence of water significantly reduced the PAH concentration in the reaction zone near the burner, which inhibited soot formation. However, the difference between the PAH concentrations for pure and emulsified fuel was small far from the burner. These results indicate that the influence of the addition of water on the PAH concentration is moderated at a furnace exit. As a result of this behavior, in the present study, the reduction in the emission of soluble organic compounds with increasing water content was more gradual than that of soot emission.

4. Discussion

It can be confirmed from the CO emission behavior shown in Fig. 13 that although the SMD increased with increasing water content ratio, the emulsified fuel combustion test at Y_w = 0.5 demonstrated stable combustion. This conflicting result is based on the effects of emulsified fuel combustion, which could induce a second atomization (micro-explosion) phenomenon in which larger droplets break up into more finely dispersed fuel droplets. Subsequently, the as-generated fine droplets undergo rapid evaporation, and the fuel vapor is then strongly mixed with air as a result of the explosion. In this way, even at high water content ratios, emulsified fuel enables complete combustion, which helps to lower the CO emissions in the exhaust gas.

However, when the same experiment was conducted at Y_w, > 0.5, the combustion was unstable because the latent heat loss due to the addition of water, which reduced the flame temperature, became too large for the fuel to burn completely. In addition, the mixture of fuel vapor with air was diluted with water vapor originating from the emulsified fuel droplets, weakening the combustion reactions.

Experimental trials have been conducted by other researchers using industrial boilers and internal combustion engines under conditions with water content ratios ranging from 0 to 0.3 [16, 36]. Emulsified fuel with a water content ratio of approximately 0.5 in these combustion systems would likely induce unstable operating conditions due to misfiring. In contrast to these previous studies [16, 36], stable combustion was successfully sustained in the present trials, even at higher water content ratios. This is likely a result of the flame holder surrounding the RIM injector. As shown in Fig. 5, fuel droplets were injected toward the inner wall of the flame holder. This configuration easily generates a recirculation zone above the injector, where hot gases are recirculated upstream, and assists evaporation and the

subsequent ignition of the fuel. As a result, combustion in the present furnace can be sustained even under high water content ratios. Unfortunately, no results are available regarding the velocity field inside the combustion furnace, so the existence of a recirculation zone in the flame holder cannot be definitively demonstrated. However, the flame holder is believed to play an important role in sustaining combustion.

In the present study, the effect of the water content ratio on NO_x emission was demonstrated. In contrast, the effects of the Reynolds and Froude numbers on NO_x emission have been investigated in many previous studies on gas combustion [33, 37, 38], which have involved scaling $EINO_x$ by the Froude and Reynolds numbers. Although these numbers are useful for representing the effects of inertia and buoyancy on NO_x production, it is difficult to individually investigate these effects on spray flames. This is because the increase in the gas velocity with increasing Reynolds and Froude numbers likely improves the atomization characteristics, which strongly affect the NO_x emissions. To identify the effect of the Reynolds and Froude numbers, it is necessary to control the diameter of the fuel droplets [39]; this remains as a task for future work.

As shown in Figs. 13, 15, and 18, NO_x and PM emissions decreased with increasing water content ratio, and excess water induced unstable combustion with high CO emissions. Therefore, the water content ratio for emulsified fuel combustion should be determined by balancing the opposing factors of emission reduction and combustion stability. In the present experimental trials, a water content ratio of 0.5 was found to be the optimal value; at this ratio, the emissions were reduced while simultaneously avoiding misfiring. However, the optimal value would vary depending on the combustion apparatus and thermal conditions. Because the proposed injector provides emulsified fuel just before injection, furnace operators can adjust the water content ratio in response to the conditions. In terms of the

balance between emission and stability, the proposed injector is considered to be suitable for practical use in industrial furnaces.

5. Summary

In this study, an RIM injector enabling the emulsification of a base fuel without any surfactant was developed, and its performance was evaluated in terms of emulsification, atomization, and the emission of NO_x and PM from a test combustion furnace. The developed injector successfully emulsified a base fuel of soybean oil at water content ratios of up to 0.5. In the proposed injector, the base fuel injected into the mixing chamber is mixed with water by the strong swirling motion of atomizing gas at the tip of swirler and is then mixed again in the thin film that attaches to the inner wall of the chamber. The emulsified fuel that is eventually discharged from the injector is a W/O emulsion.

The emulsification deteriorates the atomization characteristics of the injector because of the decrease in the mass flow ratio of atomizing gas to liquid and the increase in its viscosity resulting from emulsification. Although the SMDs of the emulsified fuel droplets exceeded 100 μm, the test combustion furnace incorporating the injector was stably operated without high CO emissions and noise at water content ratios below 0.5. NO_x and PM emissions could be simultaneously reduced by increasing the water content ratio, as when using conventional emulsified fuels. The results obtained from combustion tests demonstrate the effectiveness of the developed injector for the simultaneous reduction of emissions while maintaining the stable operation of combustion furnace.

Declarations of interest

None

Appendix A. Supplementary data

Supplementary data to this article can be found online at https://doi.org/10.1016/j.energy.2018.10.182.

References

[1] Cavaliere A, Joannon MD. Mild combustion. Progress in Energy and Combustion Science 2004; 30(4): 329-366. https://doi.org/10.1016/j.pecs.2004.02.003.

[2] Kukkadapu G, Kumar K, Sung CJ, Mehl M, Pitz WJ. Autoignition of gasoline surrogates at low temperature combustion conditions. Combustion and Flame 2015; 162(5): 2272-2285. https://doi.org/10.1016/j.combustflame.2015.01.025.

[3] Seepana S, Jayanti S. Flame structure investigations of oxy-fuel combustion. Fuel 2012; 93: 52-58. https://doi.org/10.1016/j.fuel.2011.07.033.

[4] Joannon MD, Langella G, Beretta F, Cavaliere A, Noviello C. Mild combustion: Process features and technological constrains. Combustion Science and Technology 2000; 153(1): 33-50. https://doi.org/10.1080/00102200008947249.

[5] Kadota T, Yamasaki H. Recent advances in the combustion of water fuel emulsion. Progress in Energy and Combustion Science 2002; 28(5): 385–404. https://doi.org/10.1016/S0360-1285(02)00005-9.

[6] Segawa D, Yamasaki H, Kadota T, Tanaka H, Enomoto H, Tsue M. Water-coalescence in an oil-in-water emulsion droplet burning under microgravity. Proceedings of the Combustion Institute 2000; 28(1): 985–990. https://doi.org/10.1016/S0082-0784(00)80305-7.

[7] Suzuki Y, Harada T, Watanabe H, Shoji M, Matsushita Y, Aoki H, Miura T. Visualization of aggregation process of dispersed water droplets and the effect of aggregation on secondary atomization of emulsified fuel droplets. Proceedings of the Combustion Institute 2011; 33(2): 2063–2070. https://doi.org/10.1016/j.proci.2010.05.115.

[8] Watanabe H, Shoji Y, Yamagaki T, Hayashi J, Akamatsu F, Okazaki K. Secondary atomization and spray flame characteristics of carbonated W/O emulsified fuel. Fuel 2016; 182: 259-265. https://doi.org/10.1016/j.fuel.2016.05.121.

[9] Mattiello M, Cosmai L, Pistone L, Beretta F, Massoli P. Experimental evidence for microexplosions in water/fuel oil emulsion flames inferred by laser light scattering. Symposium (International) on Combustion 1992; 24(1): 1573–1578. https://doi.org/10.1016/S0082-0784(06)80183-9.

[10] Nazha MAA, Crookes RJ. Effect of water content on pollutant formation in a burning spray of water-in-diesel fuel emulsion. Symposium (International) on Combustion 1985; 20(1): 2001–2010. https://doi.org/10.1016/S0082-0784(85)80700-1.

[11] Tsue M, Segawa D, Kadota T, Yamasaki H. Observation of sooting behavior in an emulsion droplet flame by planar laser light scattering in microgravity. Symposium (International) on Combustion 1996; 26(1): 1251-1258. https://doi.org/10.1016/S0082-0784(96)80342-0.

[12] Koziński JA. PACs formation and interaction in semipractical flames of liquid fuels. Combustion and Flame 1994; 96(3): 249–260. https://doi.org/10.1016/0010-2180(94)90012-4.

[13] Jahani H, Gollahalli SR. Characteristics of burning Jet A fuel and Jet A fuel-water emulsion sprays. Combustion and Flame 1980; 37: 145–154. https://doi.org/10.1016/0010-2180(80)90081-4.

[14] Ballester JM, Fueyo N, Dopazo C. Combustion characteristics of heavy oil-water emulsions. Fuel 1996; 75(6): 695–705. https://doi.org/10.1016/0016-2361(95)00309-6.

[15] Kozinski JA, Guthrie RIL, Slupek St. Reduction of Gaseous pollutant emissions from liquid fuel flames. International Journal of Energy, Environment, and Economics 1991; 1(1): 81-93.

[16] Chelemuge, Namioka T, Yoshikawa K, Takeshita M, Fujiwara K. Commercial-scale demonstration of pollutant emission reduction and energy saving for industrial boilers by

employing water/oil emulsified fuel. Applied Energy 2012; 93: 517–522. https://doi.org/10.1016/j.apenergy.2011.12.018.

[17] Liu F, Guo H, Smallwood GJ, Gülder, ÖL. The chemical effects of carbon dioxide as an additive in an ethylene diffusion flame: Implications for soot and NO_x formation. Combustion and Flame 2001; 125(1–2): 778–787. https://doi.org/10.1016/S0010-2180(00)00241-8.

[18] Dryer FL. Water addition to practical combustion systems - Concepts and applications. Symposium (International) on Combustion 1977; 16(1): 279–295. https://doi.org/10.1016/S0082-0784(77)80332-9.

[19] Shoji M, Yamamoto T, Tanno S, Aoki H, Miura T. Modeling study of homogeneous NO and N_2O formation from oxidation of HCN in a flow reactor. Energy 2005; 30: 337-345. https://doi.org/10.1016/j.energy.2004.04.017.

[20] Ghannam MT, Selim, MYE. Stability behavior of water-in-diesel fuel emulsion. Petroleum Science and Technology 2009; 27(4): 396–411. https://doi.org/10.1080/10916460701783969.

[21] Lin CY, Chen LW. Emulsification characteristics of three- and two-phase emulsions prepared by the ultrasonic emulsification method. Fuel Processing Technology 2006; 87(4): 309-317. https://doi.org/10.1016/j.fuproc.2005.08.014.

[22] Spadaccini LJ, Pelmas R. Evaluation of oil/water emulsions for gas turbine engines. In: Zung JT, editor. Evaporation-Combustion of Fuels; American Chemical Society: 1978, p. 232-244.

[23] Adam A, Inukai N, Kidoguchi Y, Miwa K, Miyashiro S. A study on droplets evaporation at diesel spray boundary during ignition delay period. SAE Technical Paper 2007; 2007-01–1893. https://doi.org/10.4271/2007-01-1893.

[24] Kint JH. A noncatalytic coating for platinum-rhodium thermocouples. Combustion and Flame 1970; 14: 279-281. https://doi.org/10.1016/S0010-2180(70)80040-2.

[25] Bradley D and Matthews K. Measurement of high gas temperatures with fine wire thermocouples. Journal of Mechanical Engineering Science 1968; 10: 299-305. https://doi.org/10.1243/JMES_JOUR_1968_010_048_02.

[26] Li Z, Wu Y, Cai C, Zhang H, Gong Y, Takeno K et al. Mixing and atomization characteristics in an internal-mixing twin-fluid atomizer. Fuel 2012; 97: 306-314. https://doi.org/10.1016/j.fuel.2012.03.006.

[27] Oshinowo T, Charles ME. Vertical two-phase flow part I. Flow pattern correlations. The Canadian Journal of Chemical Engineering 1974; 52: 25-35. https://doi.org/10.1002/cjce.5450520105.

[28] Li Z, Wu Y, Yang H, Cai C, Zhang H, Hashiguchi K et al. Effect of liquid viscosity on atomization in an internal-mixing twin-fluid atomizer. Fuel 2013; 103: 486-494. https://doi.org/10.1016/j.fuel.2012.06.097.

[29] Lal S, Kushari A, Gupta M, Kapoor JC, Maji S. Experimental study of an air assisted mist generator. Experimental Thermal and Fluid Science 2010; 34(8): 1029-1035. https://doi.org/10.1016/j.expthermflusci.2010.03.006.

[30] Mlkvik M, Stähle P, Schuchmann HP, Gaukel V, Jedelsky J, Jicha M. Twin-fluid atomization of viscous liquids: The effect of atomizer construction on breakup process, spray stability and droplet size. International Journal of Multiphase Flow 2015; 77: 19-31. https://doi.org/10.1016/j.ijmultiphaseflow.2015.06.010.

[31] Pal R. Evaluation of theoretical viscosity models for concentrated emulsions at low capillary numbers. Chemical Engineering Journal 2001; 81: 15-21. https://doi.org/10.1016/S1385-8947(00)00174-1.

[32] Matsui Y, Kamimoto T, and Matsuoka S. A study on the time and space resolved measurement of flame temperature and soot concentration in a D. I. Diesel engine by the two-color method. SAE Technical Paper 1979; 790491. https://doi.org/10.4271/790491.

[33] Turns SR, Myhr FH. Oxides of nitrogen emissions from turbulent jet flames: Part I-Fuel effects and flame radiation. Combustion and Flame 1991; 87(3-4): 319–335. https://doi.org/10.1016/0010-2180(91)90116-S.

[34] Jacques MT, Jordan JB, Williams A, Hadley-Coates L. The combustion of water-in-oil emulsions and the influence of asphaltene content. Symposium (International) on Combustion 1977; 16(1): 307-319. https://doi.org/10.1016/S0082-0784(77)80334-2.

[35] Furuhata T, Kobayashi Y, Hayashida K, Arai M. Behavior of PAHs and PM in a diffusion flame of paraffin fuels. Fuel 2012; 91: 16-25. https://doi.org/10.1016/j.fuel.2011.07.014.

[36] Zhang W, Chen Z, Shen Y, Shu G, Chen G, Xu B et al. Influence of water emulsified diesel and oxygen-enriched air on diesel engine NO-smoke emissions and combustion characteristics. Energy 2013; 55: 369-377. https://doi.org/10.1016/j.energy.2013.03.042.

[37] Turns SR. Understanding NO_x formation in nonpremixed flames: Experiments and modeling. Progress in Energy and Combustion Science 1995; 21: 361-385. https://doi.org/10.1016/0360-1285(94)00006-9.

[38] Meunier Ph, Costa M, Carvalho MG. On NO_x emissions from turbulent propane diffusion flames. Combustion and Flame 1998; 112: 221-230. https://doi.org/10.1016/S0010-2180(97)81770-1.

[39] Hayashi J, Watanabe H, Kurose R, Akamatsu F. Effects of fuel droplet size on soot formation in spray flames formed in a laminar counterflow. Combustion and Flame 2011; 158: 2559-2568. https://doi.org/10.1016/j.combustflame.2011.05.015.

Table 1 Characteristics of the tested fuel (soybean oil).

Property	**Value**	
Density at 25 °C	892	kg/m^3
Kinematic viscosity at 25 °C	52	mm^2/s
Flash point	230	°C
Pour point	-10	°C
Higher heating value	39.92	kJ/kg
Elemental composition		
C	77.5	wt.%
H	11.5	wt.%
O	11.0	wt.%
H/C	1.78	mol/mol
O/C	0.11	mol/mol

Figure Captions

Figure 1 (a) Cross-sectional and (b) exploded-view schematics of proposed fuel–water RIM injector.

Figure 2 Experimental apparatus for droplet size measurements using shadowgraph method.

Figure 3 Correlation between diameters of glass balls evaluated using shadowgraph method and their actual diameters.

Figure 4 Experimental apparatus for NO_x and soot emission measurements.

Figure 5 Schematic of flame holder and position of temperature measurement by thermocouples (units: mm).

Figure 6 Microscopic images of emulsified fuel droplets sampled by immersion method with (a) $Y_w = 0$, (b) $Y_w = 0.3$, (c) $Y_w = 0.5$, and (d) $Y_w = 0.7$.

Figure 7 Images of transparent mixing chamber when only base fuel was introduced. (a) Cross-sectional schematic of injector. The location of the photographed region is indicated by a broken line. (b) Series of successive images at time intervals of 48 ms (see also **Supplementary video 1**).

Figure 8 Same as Fig. 7 at $Y_w = 0.3$ (see also **Supplementary video 2**).

Figure 9 Same as Fig. 7 at $Y_w = 0.3$ with mixing chamber dismounted from main body of the injector (see also **Supplementary video 3**).

Figure 10 Droplets discharged from injector without mixing chamber dismounted at $Y_w = 0.3$.

Figure 11 Variation in droplet diameter with respect to water content ratio. (a) Probability distributions of droplet diameter. (b) SMD as a function of water content ratio and GLR.

Figure 12 Fuel viscosity plotted against fuel temperature.

Figure 13 CO emission plotted against water content ratio.

Figure 14 Photographic images of flame at (a) $Y_w = 0$ and (b) $Y_w = 0.3$.

Figure 15 NO_x emission as a function of the water content ratio.

Figure 16 Vertical temperature distributions at different water content ratios.

Figure 17 Radial temperature distributions at vertical distance of 42 mm from injection hole at different water content ratios.

Figure 18 Mass concentrations of PM, SOLID, and the SOF as functions of the water content ratio.

Figure 19 TEM images of PM at (a) $Y_w = 0$, (b) $Y_w = 0.5$.

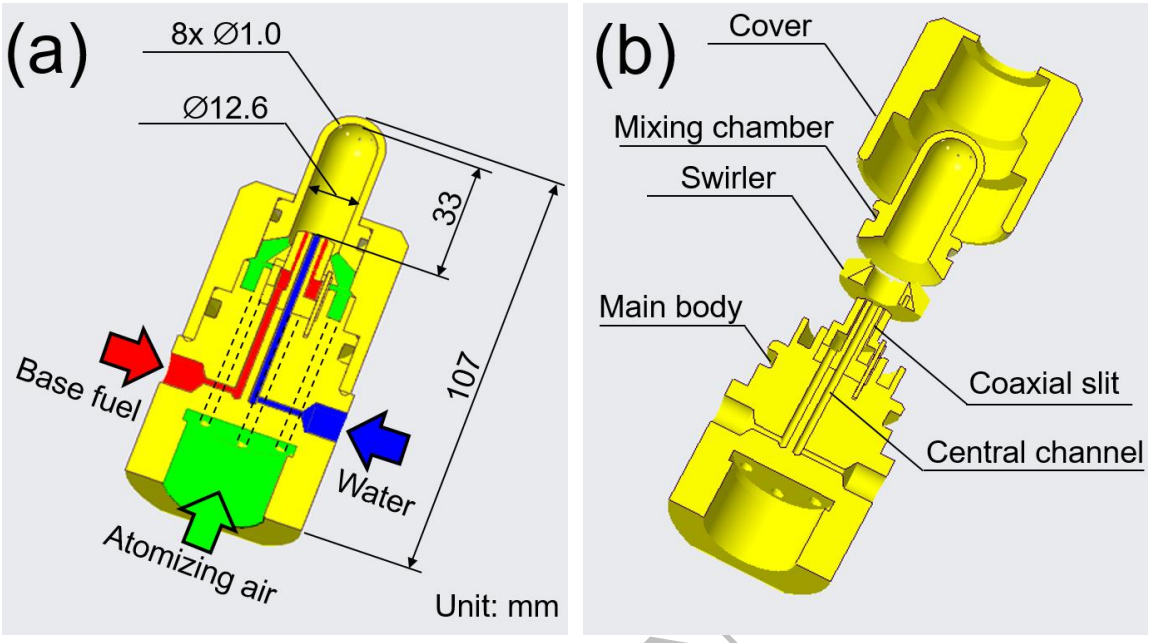

Fig. 1 (a) Cross-sectional and (b) exploded-view schematics of proposed fuel–water RIM injector.

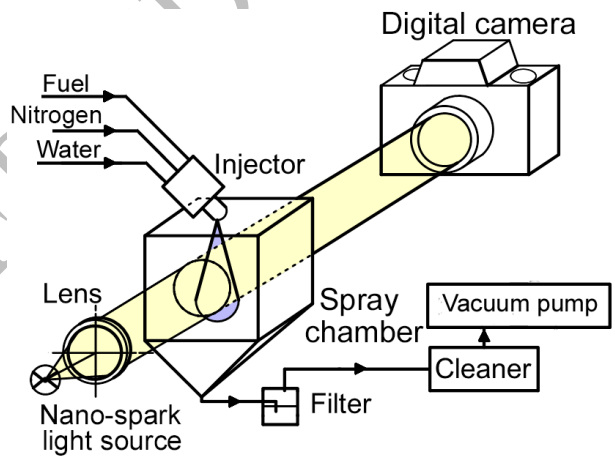

Fig. 2 Experimental apparatus for droplet size measurements using shadowgraph method.

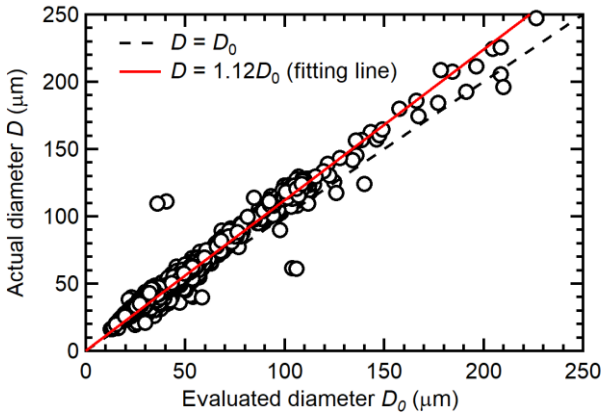

Fig. 3 Correlation between diameters of glass balls evaluated using shadowgraph method and their actual diameters.

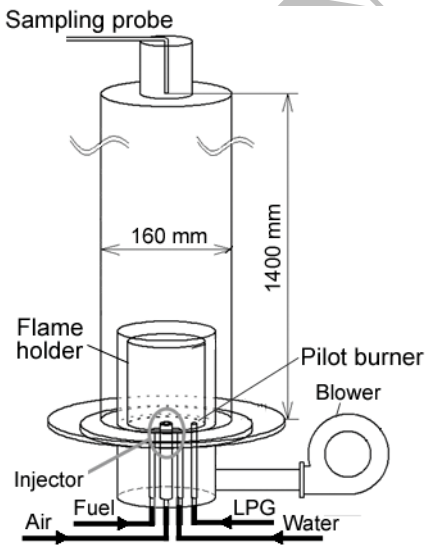

Fig. 4 Experimental apparatus for NO_x and soot emission measurements.

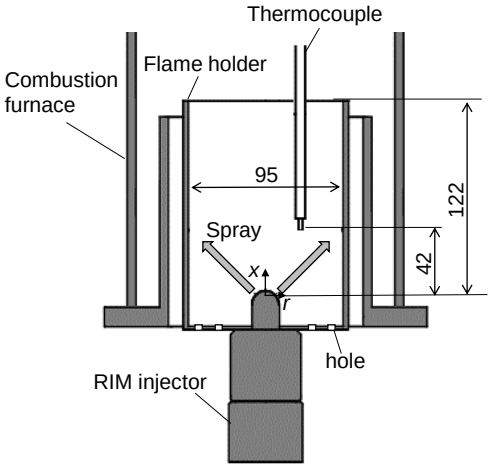

Fig. 5 Schematic of flame holder and position of temperature measurement by thermocouples (units: mm).

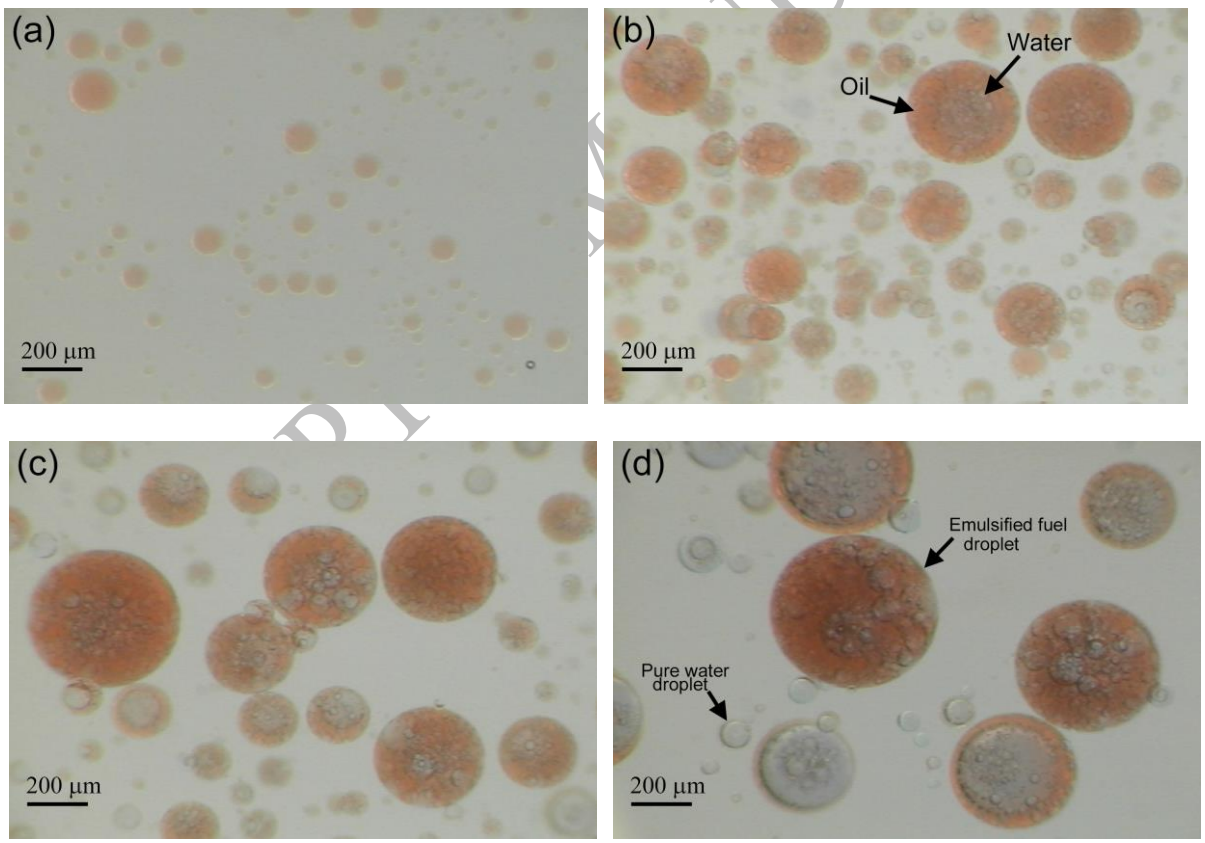

Fig. 6 Microscopic images of emulsified fuel droplets sampled by immersion method with (a) $Y_w = 0$, (b) $Y_w = 0.3$, (c) $Y_w = 0.5$, and (d) $Y_w = 0.7$.

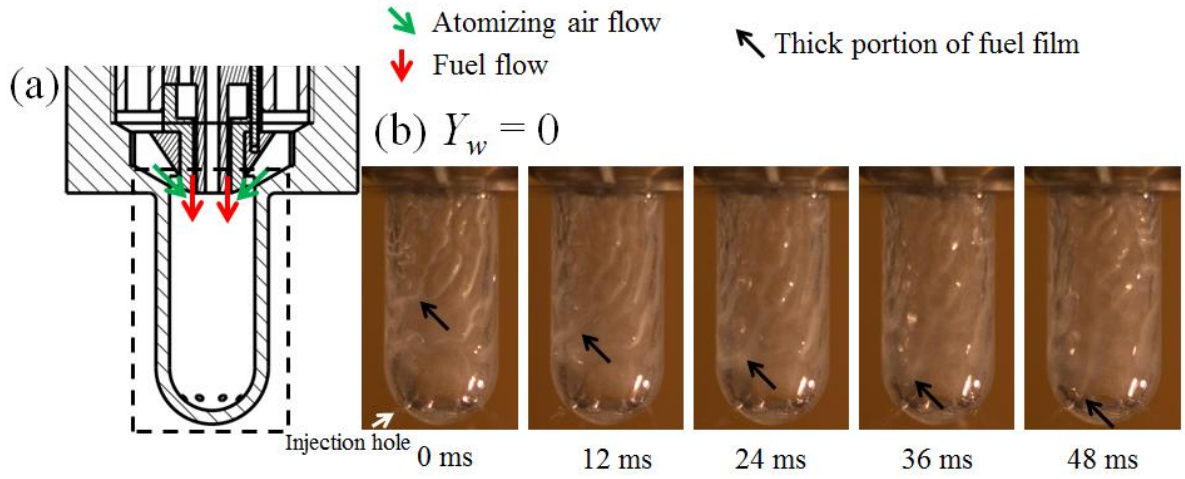

Fig. 7 Images of transparent mixing chamber when only base fuel was introduced. (a) Cross-sectional schematic of injector. The location of the photographed region is indicated by a broken line. (b) Series of successive images at time intervals of 48 ms (see also **Supplementary video 1**).

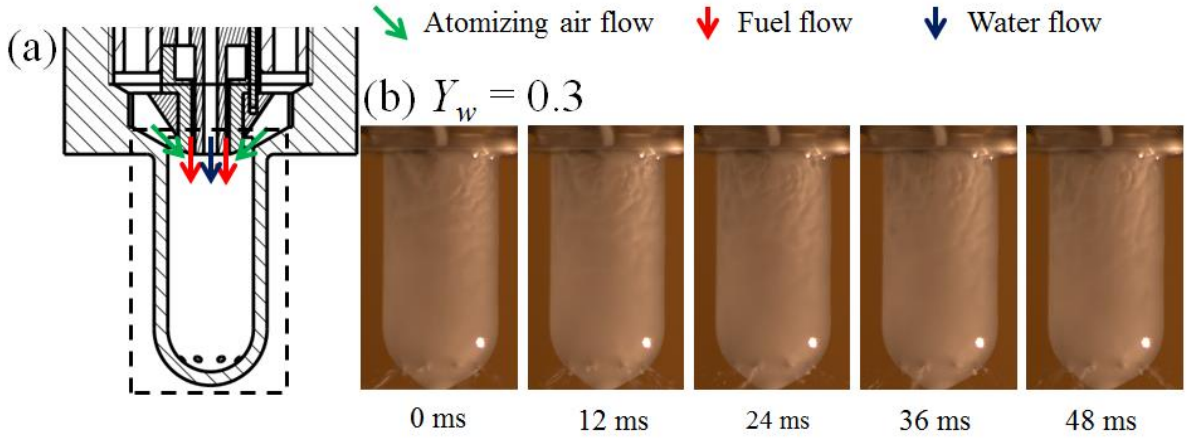

Fig. 8 Same as Fig. 7 at $Y_w = 0.3$ (see also **Supplementary video 2**).

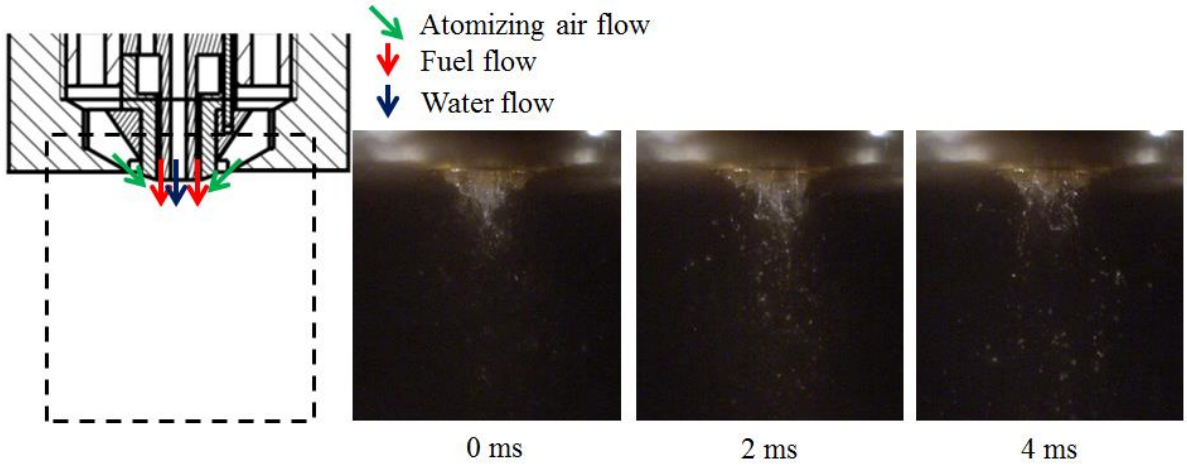

Fig. 9 Same as Fig. 7 at Y_w = 0.3 with mixing chamber dismounted from main body of the injector (see also **Supplementary video 3**).

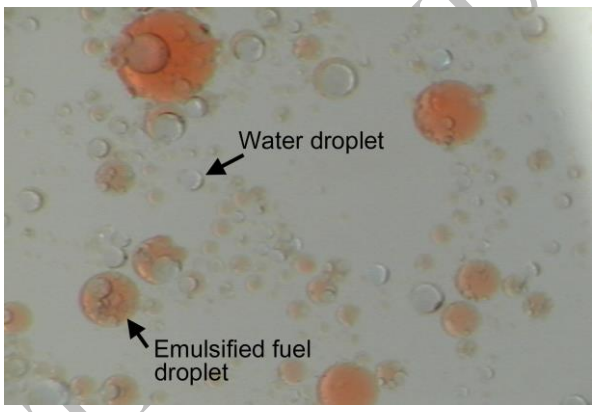

Fig. 10 Droplets discharged from injector without mixing chamber dismounted at Y_w = 0.3.

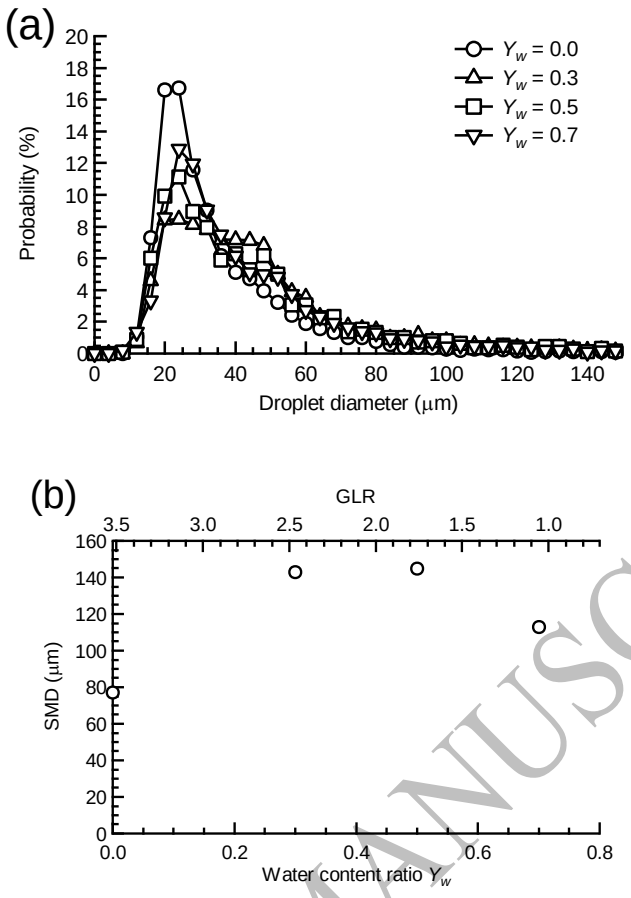

Fig. 11 Variation in droplet diameter with respect to water content ratio. (a) Probability distributions of droplet diameter. (b) SMD as a function of water content ratio and GLR.

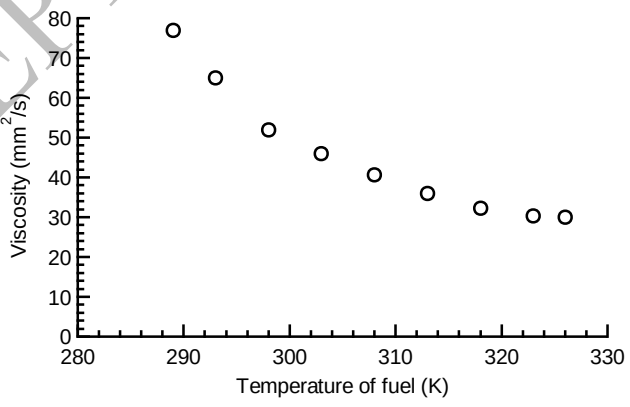

Fig. 12 Fuel viscosity plotted against fuel temperature.

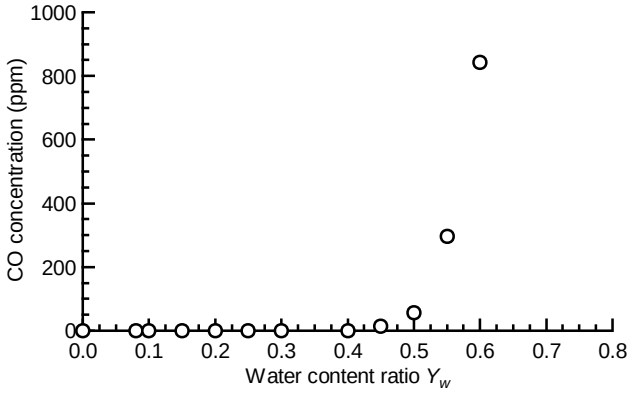

Fig. 13 CO emission plotted against water content ratio.

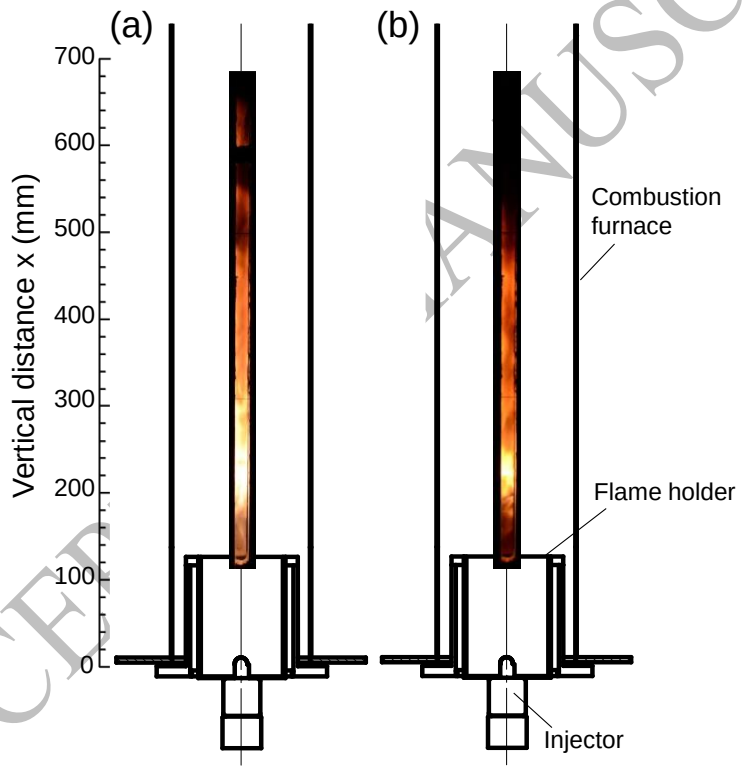

Fig. 14 Photographic images of flame at (a) $Y_w = 0$ and (b) $Y_w = 0.3$.

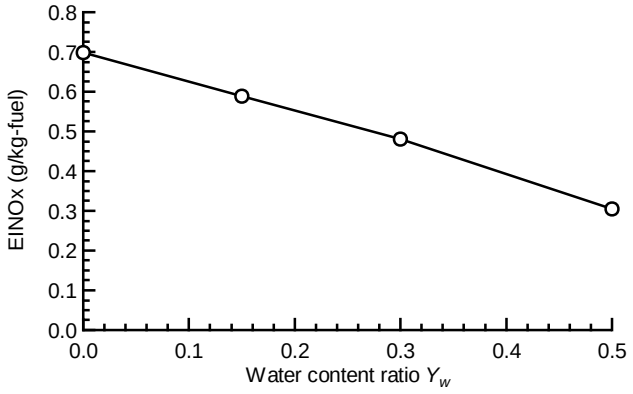

Fig. 15 NO_x emission as a function of the water content ratio.

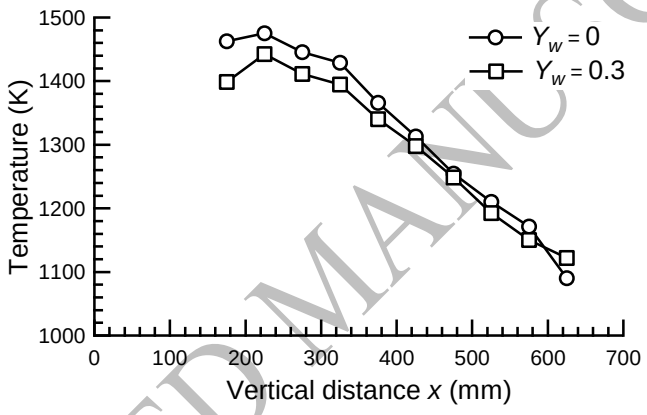

Fig. 16 Vertical temperature distributions at different water content ratios.

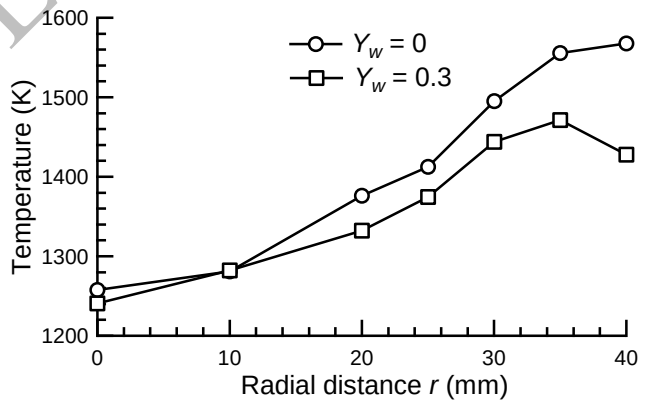

Fig. 17 Radial temperature distributions at vertical distance of 42 mm from injection hole at different water content ratios.

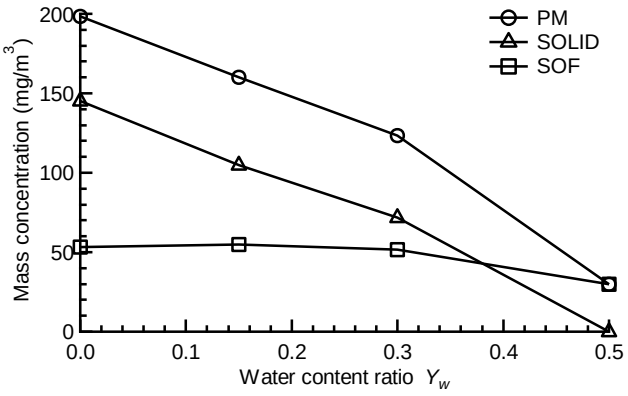

Fig. 18 Mass concentrations of PM, SOLID, and the SOF as functions of the water content ratio.

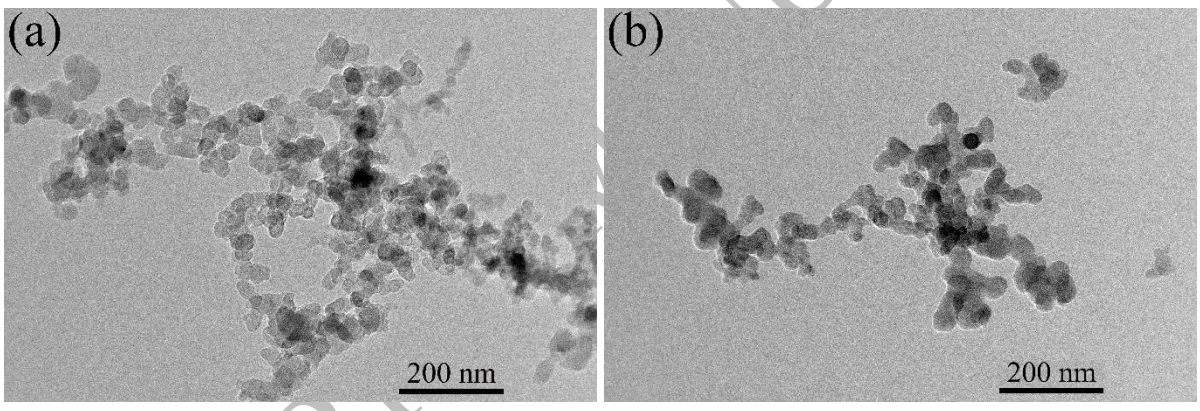

Fig. 19 TEM images of PM at (a) $Y_w = 0$, (b) $Y_w = 0.5$.

Highlights

- No surfactant is required in the fuel-water rapid internal mixing injector.
- Successful emulsification was observed in the mixing chamber.
- The NO_x and soot emissions were reduced simultaneously.